Capture of the [Mo3S4](4+) Cluster within a {Mo-18} Macrocycle Yielding a Supramolecular Assembly Stabilized by a Dynamic H-Bond Network

10 AUTHORS, INCLUDING:

Corine Simonnet-Jégat
Université de Versailles Saint-Quentin

38 PUBLICATIONS **292** CITATIONS

Jérome Marrot
French National Centre for Scientific Resea…

384 PUBLICATIONS **7,689** CITATIONS

Rosa ngo biboum
University of Tours

30 PUBLICATIONS **821** CITATIONS

Bineta Keita
Université Paris-Sud 11

280 PUBLICATIONS **8,368** CITATIONS

Capture of the [Mo$_3$S$_4$]$^{4+}$ Cluster within a {Mo$_{18}$} Macrocycle Yielding a Supramolecular Assembly Stabilized by a Dynamic H-Bond Network

Sylvain Duval,[†] Sébastien Floquet,[†] Corine Simonnet-Jégat,[†] Jérôme Marrot,[†] Rosa Ngo Biboum,[‡] Bineta Keita,*[‡] Louis Nadjo,[‡] Mohamed Haouas,[†] Francis Taulelle,[†] and Emmanuel Cadot*[†]

Institute Lavoisier of Versailles, University of Versailles Saint Quentin, 45 avenue des Etats Unis, 78035 Versailles Cedex, France, and Laboratoire de Chimie Physique, UMR 8000, Université de Paris-Sud, 91405 Orsay Cedex, France

Received November 17, 2009; E-mail: cadot@chimie.uvsq.fr; bineta.keita@u-psud.fr

Abstract: The use of the [Mo$_3$S$_4$(Hnta)$_3$]$^{2-}$ complex (nta^{3-} = nitrilotriacetate) as structuring agent toward the self-condensation process of the [Mo$_2$O$_2$S$_2$(OH$_2$)$_6$]$^{2+}$ cation leads to the largest oxothiomolybdenum ring. In the solid state, X-ray diffraction analysis reveals the presence of the targeted molecular compound (noted **1a**), which consists of the {Mo$_{18}$O$_{18}$S$_{18}$(OH)$_{18}$} host templated by the [Mo$_3$S$_4$(Hnta)$_3$]$^{2-}$ guest. Nevertheless, the structure shows an additional molecular moiety corresponding to a dinuclear unit {Mo$_2$O$_2$S$_2$} coordinated to two nta^{3-} ligands, mutually arranged in a cis fashion (**1b**). In the solid state, both entities interact through two short hydrogen bonds to give a striking supramolecular adduct, noted {**1a**−**1b**}. Synthetic procedures to prepare the individual species as pure compounds were reported. **1a** was obtained as a pure mixed Cs$^+$/NMe$_4^+$ salt while the dinuclear unit [Mo$_2$O$_2$S$_2$(Hnta)$_2$]$^{2-}$ was obtained as mixed K$^+$/Na$^+$ crystals. X-ray diffraction study of the latter reveals a trans isomer (noted **1b′**), characterized by the specific coordination of both nta^{3-} ligands. All the compounds were characterized in solution (D$_2$O or DMSO) by multiexperiment ^{1}H NMR (1D, COSY, NOESY, and DOSY). The overall results were consistent with the retention of the adduct {**1a**−**1b**} which exhibits a supramolecular reactivity. The dinuclear individual species in solution gave rise to cis−trans equilibrium, while in the presence of the oxothiomolybdenum ring **1a**, the dinuclear unit is maintained as a frozen cis complex. DOSY NMR provides a definitive argument for the integrity of the supramolecular assembly. In addition, preliminary electrochemical study of **1a** is also reported.

Introduction

The design and synthesis of nanoscopic inorganic clusters containing a large number of metal centers represent an enduring challenge for the chemist. In this way, polyoxometalate compounds (POMs) are potentially attractive for the design of large assemblies with targeted synergistic functionalities[1] and promising applications in diverse fields of science, such as catalysis, medicine, and material sciences.[2] Furthermore, POMs have attracted attention as unique building blocks for supramolecular inorganic systems. In this context, hydrolytic condensation of the {Mo$_2$O$_2$S$_2$(OH$_2$)$_6$}$^{2+}$ aqua ion has produced a striking

subclass of compounds, namely the cyclic oxothiomolybdates.[3] Using the concepts of the templated synthesis, numerous {Mo$_2$O$_2$S$_2$} based molecules with controlled nuclearity, shape, and symmetry have been isolated and characterized as host−guest assemblies. Systematic investigations demonstrate that two types of interactions govern the host−guest stability. Using basic ions such as polycarboxylate, (poly)phosphate, or metalates ions, the host and the guest components are associated through direct covalent interactions[4] while the presence of weak bases such as halides[5] or sulfonate ions[6] leads to fragile arrangements built on weak H-bond interactions involving polarized inner water molecules. This class of compounds exhibits a rare flexibility property at the origin of unusual host−guest dynamics, mainly orchestrated by the mutual adaptability between both compo-

† University of Versailles Saint Quentin.
‡ Université de Paris-Sud.

(1) (a) Song, Y. F.; McMillan, N.; Long, D. L.; Thiel, J.; Ding, Y. L.; Chen, H. S.; Gadegaard, N.; Cronin, L. *Chem.—Eur. J.* **2008**, *14*, 2349. (b) Geletii, Y. V.; Botar, B.; Kögerler, P.; Hillesheim, D. A.; Musaev, D. G.; Hill, C. L. *Angew. Chem., Int. Ed.* **2008**, *47*, 3896.

(2) (a) Pope, M. T., Müller, A., Eds. *Polyoxometalates: From Platonic Solids to Anti Retroviral Activity*; Kluwer Academic: Dordrecht, 1994. (b) Pope, M. T., Müller, A., Eds. *Polyoxometalate Chemistry: From Topology via Self-Assembly to Applications*; Kluwer Academic: Dordrecht, 2001. (c) Yamase, T.; Pope, M. T. *Nanostructure Science and Technology*; Springer: Heidelberg, 2002; Vol. 2. (d) Borrás-Almenar, J. J.; Coronado, E.; Müller, A.; Pope, M. T. *Polyoxometalate Molecular Science*; Kluwer Academic: Dordrecht, 2003.

(3) (a) Cadot, E.; Salignac, B.; Halut, S.; Sécheresse, F. *Angew. Chem., Int. Ed.* **1998**, *37*, 611. (b) Cadot, E.; Sécheresse, F. *Chem. Commun.* **2002**, 2189. (c) Lemonnier, J.-F.; Floquet, S.; Marrot, J.; Terazzi, E.; Piguet, C.; Lesot, P.; Pinto, A.; Cadot, E. *Chem.—Eur. J.* **2007**, *13*, 3548.

(4) (a) Cadot, E.; Pouet, M. J.; Robert-Labarre, C. R.; du Peloux, C.; Marrot, J.; Sécheresse, F. *J. Am. Chem. Soc.* **2004**, *126*, 9127. (b) Salignac, B.; Riedel, S.; Dolbecq, A.; Sécheresse, F.; Cadot, E. *J. Am. Chem. Soc.* **2000**, *122*, 10381.

(5) Cadot, E.; Salignac, B.; Marrot, J.; Dolbecq, A.; Secheresse, F. *Chem. Commun.* **2000**, 261.

(6) Lemonnier, J. F.; Floquet, S.; Marrot, J; Cadot, E. *Eur. J. Inorg. Chem.* **2009**, *34*, 5233.

nents.[7,3a] Besides, not only platonic materials, the $\{Mo_2O_2S_2\}$-based systems have been revealed to function as efficient bioinspired electrocatalysts toward the reduction of protons into hydrogen (HER) at very low overpotentials.[8] Trends in electrocatalytic properties for this class of molecular materials are not still well understood, but their chemical potentialities such as the diversity of the host−guest combinations offer some relevant optimization perspectives. One idea consists of including stereospecifically electroactive components within the Mo ring for synergistic functionalities such as electron (or protons) storage and transfer. The tremendous propensity of the Mo rings to encapsulate polycarboxylate ions prompts us to use the $[Mo_3S_4(Hnta)_3]^{2-}$ ion as guest component (nta^{3-} = nitrilotriacetate).[9] This complex possesses three hanging carboxylic groups able to act as three anchoring points.[10,11] The encapsulation of the electrochemically active $\{Mo_3S_4\}$ core opens the route toward hierarchical mixed-valence $Mo^V/Mo^{IV}/Mo^{III}$ rings, chemically able to coordinate additional metallic centers such as Pd^{2+}, Ni^{2+}, or Fe^{2+}, potentially attractive for their coordinative and redox properties.[12] Herein, we report on a mixed Mo-cluster derivative which exhibits a $\{Mo_3S_4\}$-based complex embedded within the largest $\{Mo_{18}\}$ wheel. Nevertheless, the encapsulation reaction proceeds through complex processes which result in the formation of a striking supramolecular assembly. Structural characterizations reveal the presence of a dinuclear anion hydrogen bonded on the hydrophilic surface of the $\{Mo_{18}\}$ ring. Full NMR studies provide evidence that, despite the weakness of the interactions, the supramolecular association is retained in solution, even in a polar solvent such as H_2O. NMR results are consistent with a labile arrangement built upon a dynamic H-bond network, probably at the origin of the supramolecular stability. Preliminary electrochemical studies are presented, showing that combination of the $\{Mo_{18}\}$ ring and the $\{Mo_3S_4\}$ induces an enhancement of the electrocatalytic behavior, whereas the intrinsic electrochemical properties of the $\{Mo_3S_4\}$ core appear almost unaffected.

Experimental Section

Synthesis of the Compounds. The precursors $Na_2[Mo_3S_4(Hnta)_3]\cdot 7H_2O$ and $K_{2-x}(NMe_4)_x[I_2Mo_{10}O_{10}S_{10}(OH)_{10}(H_2O)_5]\cdot 20H_2O$ were synthesized according to published procedures.[3,10] All others reagents were used as purchased without further purification.

$K_9\{[Mo_{18}O_{18}S_{18}(OH)_{18}(H_2O)_9(Mo_3S_4(nta)_3)][Mo_2O_2S_2(nta)_2]\}\cdot 45H_2O$, $1\equiv K_9\text{-}\{1a\text{−}1b\}\cdot 45H_2O$. $Na_2[Mo_3S_4(Hnta)_3]\cdot 7H_2O$ (0.24 g, 0.21 mmol) and $K_{2-x}(NMe_4)_x[I_2Mo_{10}O_{10}S_{10}(OH)_{10}(H_2O)_5]\cdot 20H_2O$ (0.9 g, 0.38 mmol) were mixed in 20 mL of water. The pH was adjusted to 4.5 with $1\ mol\cdot L^{-1}$ KOH aqueous solution. The resulting dark-green solution was heated at 40 °C for 45 min. After cooling, the solution was filtered, and KCl (3 g) was added, provoking the

precipitation of a green solid ($\sim$0.2 g) which was removed by filtration. The resulting clear solution was kept in air for slow evaporation. After a few days, dark-green crystals of **1** deposited and were isolated by filtration, washed by cold water, and dried in air. Yield: 0.18 g (16% based on Mo). IR (KBr): $\bar{\nu}$ (cm^{-1}) = 1625 (vs), 1570 (sh), 1450 (w), 1419 (m), 1384 (m), 1320 (w), 947 (s), 511 (s). Elemental analysis (%) calcd for $C_{30}H_{156}K_9Mo_{23}N_5O_{122}S_{24}$ (**1**, MM = 5867.4 $g\cdot mol^{-1}$): C 6.14; H 2.68; N 1.19; S 13.12; K 5.99; Mo 37.61. Found: C 6.04; H 2.51; N 1.16; S 12.89; K 5.98; Mo 36.20.

$Cs_{4.7}(NMe_4)_{0.3}[Mo_{18}O_{18}S_{18}(OH)_{18}(H_2O)_9(Mo_3S_4(nta)_3)]\cdot 36H_2O$, $2\equiv Cs_{4.7}(NMe_4)_{0.3}\text{-}1a\cdot 36H_2O$. The procedure is quite similar to that used for **1**, employing CsCl instead of KCl. The cesium salt was precipitated by addition of CsCl (0.40 g, 2.4 mmol). The crystalline product of **2** was not available. Yield: 1.15 g (93%). IR (KBr) for **2**: $\bar{\nu}$ (cm^{-1}) = 1617 (vs), 1576 (sh), 1484 (w, NMe_4^+), 1415 (m), 1379 (m), 1318 (w), 948 (s), 516 (m). Elemental analysis (%) Calcd for $C_{19.2}Cs_{4.7}H_{129.5}Mo_{21}N_{3.3}O_{99}S_{22}$ (**2**, MM = 5334.8 $g\cdot mol^{-1}$): C 4.32; H 2.45; N 0.87; S 13.22; Mo 37.75; Cs 11.71. found: C 4.41; H 2.23; N 1.01; S 12.93; Mo 36.94; Cs 11.91.

$KNa[Mo_2O_2S_2(Hnta)_2]\cdot 7H_2O$, $3\equiv KNa\text{-}1b'\cdot 7H_2O$. $K_{2-x}(NMe_4)_x\text{-}[I_2Mo_{10}O_{10}S_{10}(OH)_{10}(H_2O)_5]\cdot 20H_2O$ (0.5 g; 0.21 mmol) and 10 mL of $1\ mol\cdot L^{-1}$ hydrochloric acid solution were suspended in 20 mL of water. Nitrilotriacetic acid (1 g; 5 mmol) (noted H_3nta) was then added to the previous solution and the pH adjusted to 3 with 1 $mol\cdot L^{-1}$ sodium hydroxide solution to give an orange solution. Potassium chloride (2 g; 27 mmol) was then added and the resulting solution kept to stand in air. Several days after, well-shaped orange-red crystals were obtained, collected by filtration, washed with cold water, ethanol and ether, and dried in air (0.75 g, yield 75% based on Mo). IR (KBr) for **3**: $\bar{\nu}$ (cm^{-1}) = 1732 (s), 1645 (vs), 1589 (vs), 1440 (m), 1425 (m), 1396 (s), 1237 (s), 1217 (m), 1111 (w), 998 (w), 928 (s), 879 (m), 772 (w), 690 (w), 538 (s), 464 (m), 411 (w). Elemental analysis (%) Calcd for $C_{12}H_{28}KMo_2N_2NaO_{19}S_2$ (**3**, MM = 854.5 $g\ mol^{-1}$): C 16.87; H 3.30; N 3.28; S 7.51; Mo 22.46; Na 2.69; K 4.58. found: C 16.67; H 3.26; N 3.15; S 7.44; Mo 22.16; Na 2.29; K 5.14.

Elemental Analyses. Elemental analyses were performed by the Service Central d'Analyses du CNRS. The water contents corresponding to the weight loss until about 250 °C were determined by thermal gravimetric analysis (TGA experiments) with a TGA-7-Perkin-Elmer apparatus.

Infrared Spectra. Infrared spectra were recorded on a FTIR Magna 550 Nicolet spectrophotometer using the technique of pressed KBr pellets.

X-ray Diffraction Studies. Crystallographic data for **1** and **3** are summarized in Table 1. Intensity data collections were carried out at room temperature with a Bruker X8 APEX2 CCD for **1** and with a Siemens SMART three-circle diffractometer equipped with a CCD bidimensional detector for **3**, using the Mo Kα wavelength (λ = 0.71073 Å). Both crystals were mounted in a sealed Lindeman tube to prevent any loss of crystallization water. An empirical absorption correction was applied using the SADABS program[13] based on the method of Blessing.[14] The structures were solved by direct methods and refined by full-matrix least-squares using the SHELX-TL package.[15] Heavier atoms (Mo) for each structure were initially located by direct methods. The remaining non-hydrogen atoms were located from Fourier differences and were refined with anisotropic thermal parameters. The disordered atoms, alkali cations, or oxygen atoms of crystallization water were isotropically refined. For **3**, among the two alkali Na and K cations found by elemental analysis, only 0.5 potassium ion were located. The remaining 0.5

(7) Lemonnier, J. F.; Floquet, S.; Kachmar, A.; Rohmer, M. M.; Bénard, M.; Marrot, J.; Terazzi, E.; Piguet, C.; Cadot, E. *Dalton Trans.* **2007**, 3043.

(8) Keita, B.; Floquet, S.; Lemonnier, J.-F.; Cadot, E.; Kachmar, A.; Bénard, M.; Rohmer, M.-M.; Nadjo, L. *J. Phys. Chem. C* **2008**, *112*, 1109.

(9) Cotton, F. A.; Llusar, R.; Marler, D. O.; Schwotzer, W. *Inorg. Chim. Acta* **1985**, *102*, L25.

(10) Shibahara, T.; Yamasaki, M.; Sakane, G.; Minami, K.; Yabuki, T.; Ichimura, A. *Inorg. Chem.* **1992**, *31*, 640.

(11) Duval, S.; Marrot, J.; Simonnet-Jégat, C.; Cadot, E. *Solid State Sci.* **2009**, *11*, 56.

(12) (a) Sokolov, M. N.; Chubarova, E. V.; Hernandez-Molina, R.; Clausen, M.; Naumov, D. Y.; Vicent, C.; Llusar, R.; Fedin, V. P. *Eur. J. Inorg. Chem.* **2005**, 2139. (b) Llusar, R.; Uriel, S. *Eur. J. Inorg. Chem.* **2003**, 1271. (c) Herbst, K.; Zanello, P.; Corsini, M.; D'amelio, N.; Dalhenburg, L.; Brorson, M. *Inorg. Chem.* **2003**, *42*, 974. (d) Shibahara, T.; Akashi, H.; Kuroya, H. *J. Am. Chem. Soc.* **1988**, *110*, 3313.

(13) Sheldrick, G. M. *SADABS, program for scaling and correction of area detector data*; University of Göttingen: Germany, 1997.

(14) Blessing, R. *Acta Crystallogr.* **1995**, *A51*, 33.

(15) Sheldrick, G. M. *Acta Crystallogr.* **1990**, *A46*, 467. Sheldrick, G. M. *SHELX-TL version 5.03, Software Package for the Crystal Structure Determination*; Siemens Analytical X-ray Instrument Division: Madison, WI, 1994.

Table 1. Relevant Crystallographic Data for **1** and **3**

	1	3
formula	$C_{30}H_{138}K_9Mo_{23}N_5O_{113}S_{24}$	$C_{24}H_{56}K_2Mo_4N_4Na_2O_{42}S_4$
M, g·mol^{-1}	5705.41	1708.91
T, K	293(2)	293(2)
crystal size (mm)	0.36 × 0.16 × 0.14	0.40 × 0.20 × 0.10
crystal system	monoclinic	tetragonal
space group	Pc	$P4/ncc$
a, Å	18.0140(2)	20.485(2)
b, Å	27.2308(5)	20.485(2)
c, Å	19.7247(3)	29.203(2)
α, deg	90	90
β, deg	92.5880(10)	90
γ, deg	90	90
V, Å^3	9665.8(3)	12254.6(14)
Z	2	8
ρ_{calc}, g·cm^{-3}	1.960	1.853
μ(Mo Kα), cm^{-1}	1.974	1.189
λ(Mo Kα), Å	0.71073	0.71073
θ range, deg	0.75−30.05	1.41−30.38
data collected	222028	91285
unique data	51875	9178
unique data $I > 2\sigma(3I)$	43437	5677
no. parameters	1888	304
R_1F^a	0.0512	0.0691
$R_w(F^2)^b$	0.1405	0.1200
GOF	1.059	1.099

^{a} $R_1 = (\sum|F_o| - |F_c|)/(\sum|F_c|)$ ^{b} $R_w = \sqrt{(\sum w(F_o^2 - F_c^2)^2)/(\sum w(F_o^2)^2)}$ (1)/ $(w) = \sigma^2 F_o^2 + (aP)^2 + bP$.

potassium and the sodium cations are probably severely disordered within the large voids observed in the structure of **3**.

Further details about of the crystal structure determinations may be obtained free of charge from the Cambridge Crystallographic Data Centre via www.ccdc.cam.ac.uk/data_request/cif on quoting the depository number CCDC-712949 and CCDC-745959 for **1** and **3**, respectively.

NMR Spectroscopy. ^{1}H NMR samples were prepared as solutions in D_2O or DMSO[d_6]. ^{1}H chemical shifts were referenced to TMS as external standard ($\delta = 0$ ppm). NMR spectra were recorded on a Bruker AMX-400 spectrometer (^{1}H at 400 MHz, 9.4 T) at room temperature using the standard Bruker software (version 2.6 of the XWIN-NMR program) and an inverse probe-head with actively shielded gradient coils. One-dimensional (1D) ^{1}H NMR spectra were acquired with 3012 Hz spectral width, 16k complex data points, 10.5 μs pulse width, 32 scans, 2.7 s acquisition time, and 2.3 s relaxation delay. The COSY experiments were obtained using a standard COSY pulse sequence,[16] with a pulsed-field-gradient mode[17] 3 G/cm gradient strength, 8k complex data points in t_2, 3012 Hz spectral width in f_2 and f_1, 32 scans per t_1 increment, 1.4 s acquisition time, 1.6 s relaxation delay, 512 t_1 increments zero-filled to 1k, unshifted sine bell window in t_1, and magnitude-mode recording and presentation. No symmetrization procedure was applied. The overall measurement time for one experiment was about 1 day. The NOESY experiments were performed using standard NOESY pulse sequence with 3012 Hz spectral width in f_2 and f_1, 8k complex data points in t_2, 512 t_1 increments zero-filled to 1k, 32 scans per t_1 increment, 1.6 s acquisition time, 1.6 s relaxation delay, and 0.5 Hz exponential line broadening in t_1 and t_2. Different mixing times were used at 0.5, 5, 50, and 500 ms. The overall measurement time for one experiment was about 1 day. Translational diffusion measurements were performed using Bruker's 'ledbpgs2s' stimulated echo DOSY pulse sequence including bipolar and spoil gradients. Sine-shaped

gradient strength was linearly incremented in 50 steps between 1% and 99% of the upper limit of 28 G/cm B_0 field gradient. The diffusion delay was always 150 ms, and the gradient pulse duration was typically 2 ms. Apparent diffusion coefficients were obtained using an adapted algorithm based on the inverse Laplace transform and maximum entropy.[18] Typical DOSY experiments lasted ~14 h with 200 acquired scans. Variable-temperature ^{1}H NMR experiments were recorded on a Bruker Avance operating at 300 MHz in 5-mm o.d. tubes.

Electrochemistry. The solutions were deaerated thoroughly for at least 30 min with pure argon and kept under a positive pressure of this gas during the experiments. The source, mounting and polishing of the glassy carbon (GC, Tokai, Japan) electrodes has been described elsewhere.[19] The glassy carbon samples had a diameter of 3 mm. Controlled potential coulometry was carried out with a large surface area glassy carbon plate. The electrochemical setup was an EG&G 273 A driven by a PC with the M270 software. Potentials are quoted against a saturated calomel electrode (SCE). The counterelectrode was platinum gauze of large surface area. All experiments were performed at room temperature. The polyoxo-metalates concentration was 1 mM or 0.2 mM. All cyclic voltam-mograms were recorded at a scan rate of 10 mV s^{-1}, unless otherwise stated. The composition of the various media were as follows for pH 5: 1 M CH_3COOLi + CH_3COOH; for pH 7: 1 M LiCl + 0.2 M tris(hydroxymethyl)aminomethane or 0.5 M Li_2SO_4 + 0.2 M tris(hydroxymethylaminomethane).

Stability Studies. Prior to any studies of the electrochemical behavior, the stability domain of **1a** over the pH scale has been determined by UV−vis spectrometry as a function of time. Spectra were recorded with a Lambda 19 Perkin-Elmer spectrophotometer. All solutions were 30 μM in polyanion and were placed in quartz cells with optical path of 1 cm. In pH 7 medium [0.5 M Li_2SO_4 + 0.2 M Tris(hydroxymethyl)aminomethane], the spectrum of **1a** was characterized by two well-defined maxima at 620 and 280 nm and by a shoulder at 356 nm (Figure S1 in Supporting Information). The spectrum of **1a** remains identical both in peak intensity and wavelength locations over a period of several hours over a pH range from 3 to 9. Such results were also confirmed by ^{1}H NMR study (not shown).

Results and Discussion

Synthesis. Direct addition of the neutral precursor [$Mo_{10}O_{10}S_{10^-}$(OH)$_{10}$(H$_2$O)$_5$] to a solution of [Mo_3S_4(Hnta)$_3$]$^{2-}$ at pH = 4.5 followed by addition of excess potassium chloride leads to the slow deposition of single-crystals of **1** in a low yield (16%). Characterization of **1** (elemental analysis, X-ray diffraction study, and multi-^{1}H NMR experiments, see below) reveals that crystals of **1** contain two distinct molecular arrangements corresponding to the targeted large cyclic cluster, i.e. {Mo$_{18}$} templated by the [Mo$_3$S$_4$(nta)$_3$]$^{5-}$ complex (**1a**), and to a basic {Mo$_2$O$_2$S$_2$}$^{2+}$ unit coordinated by two nta^{3-} ligands (**1b**), K$_9${[Mo$_{18}$O$_{18}$S$_{18}$(OH)$_{18}$(H$_2$O)$_9$(Mo$_3$S$_4$(nta)$_3$)][Mo$_2$O$_2$S$_2$(nta)$_2$]}· 45H$_2$O **1**≡K$_9$-{**1a**−**1b**}·45H$_2$O. Such a result indicates that ligand exchange reactions and hydrolytic cleavage occur simultaneously in solution. Such processes appear to be favored by the presence of potassium since whatever the conditions of isolation of the solid, either rapid precipitation or long time crystallization, the presence of the dinuclear complex **1b** was always detected by ^{1}H NMR. Nevertheless, an alternative procedure to synthesize pure **1a** assembly has been carried out that avoids the presence of excess potassium ions. The targeted {Mo$_{18}$-[Mo$_3$S$_4$(nta)$_3$]}$^{5-}$ anion (**1a**) was obtained pure in a high yield (93%) as a mixed Cs$^+$-NMe$_4^+$ salt,

(16) (a) Aue, W. P.; Bartholdi, E.; Ernst, R. R. *J. Chem. Phys.* **1975**, *64*, 2229. (b) Braun, S.; Kalinowski, H.-O.; Berger, S. *150 and More Basic NMR Experiments*; Wiley-VCH: Weinheim, 1998; p 353.

(17) (a) von Kienlin, M.; Moonen, C. T.; van der Toorn, A.; van Zijl, P. C. M. *J. Magn. Reson.* **1991**, *93*, 423. (b) Braun, S.; Kalinowski, H.-O.; Berger, S. *150 and More Basic NMR Experiments*; Wiley-VCH: Weinheim, 1998; p 477.

(18) Delsuc, M. A.; Malliavin, T. E. *Anal. Chem.* **1998**, *70*, 2146.

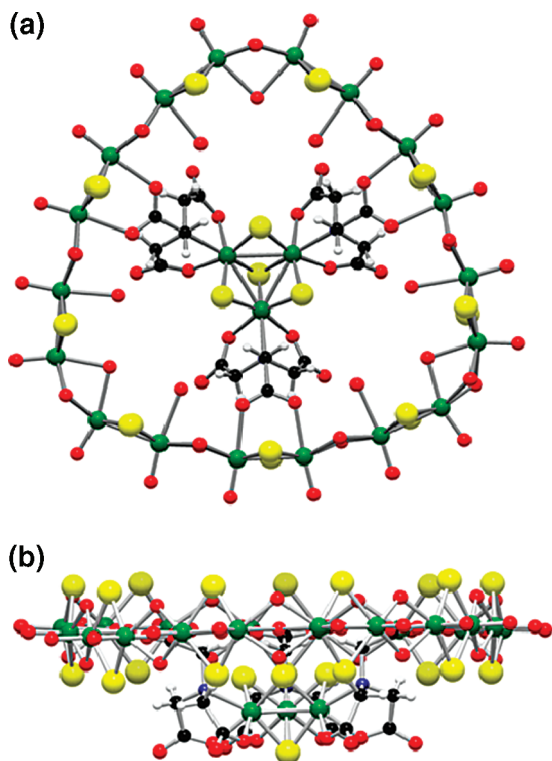(19) Keita, B.; Nadjo, L. *J. Electroanal. Chem.* **1988**, *243*, 87.

Figure 1. Ball-and-stick representations of **1a**. (a) Top-view in the direction of the C_3 axis. (b) Side view highlighting the location of the anchored {Mo$_3$S$_4$} cluster above the {Mo$_{18}$} ring. (Color code: green spheres, Mo; yellow spheres, S; red spheres, O; black spheres, C; white spheres, H.)
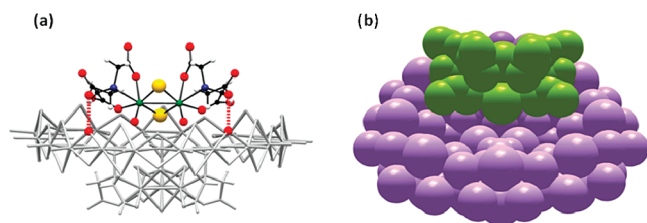

Figure 2. Two representations of the supramolecular adduct {**1a**−**1b**}; (a) highlighting the two H-bonds between the hanging carboxylate groups of **1b** (ball-and-stick representation) and the surface of the {Mo$_{18}$} ring of **1a** (gray sticks representation); (b) space-filling representation showing the supramolecular host−guest arrangement where the component **1b** (green spheres) partially fills the widened open basket **1a** (violet spheres).

Cs$_{4.7}$(NMe$_4$)$_{0.3}$[Mo$_{18}$O$_{18}$S$_{18}$(OH)$_{18}$(H$_2$O)$_9$(Mo$_3$S$_4$(nta)$_3$)]·36H$_2$O, **2**≡Cs$_{4.7}$(NMe$_4$)$_{0.3}$−**1a**·36H$_2$O.

Structure of the Anions. {[Mo$_{18}$O$_{18}$S$_{18}$(OH)$_{18}$(H$_2$O)$_9$(Mo$_3$S$_4$-(nta)$_3$)][Mo$_2$O$_2$S$_2$(nta)$_2$]}$^{9-}$ ({1a−1b}). X-ray crystallographic analysis of **1** reveals the presence of two discrete anionic entities labeled **1a** and **1b**. The molecular structure of **1a** consists of the targeted host−guest arrangement comprising the largest {Mo$_{18}$O$_{18}$S$_{18}$(OH)$_{18}$(OH$_2$)$_9$} wheel of about 20 Å in diameter (abbreviated {Mo$_{18}$} hereafter) containing an embedded [Mo$_3$S$_4$(nta)$_3$]$^{5-}$ complex (Figure 1). The structure of the other molecular component, **1b**, corresponds to a dinuclear unit [Mo$_2$O$_2$S$_2$(nta)$_2$]$^{2+}$ symmetrically coordinated by two nta^{3-} ligands through the nitrogen and oxygen atoms of two acetate groups. However, both the nitrogen atoms are disposed in a cis arrangement, where the two uncoordinated acetate groups lie down on the same side of the complex (Figures 2 and 3a). The inorganic ring {Mo$_{18}$} is built up from direct connections of nine dinuclear units {Mo$_2$O$_2$S$_2$} linked by double hydroxo
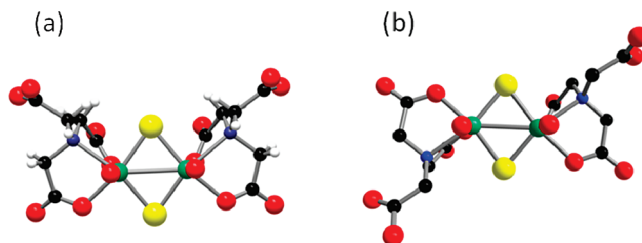

Figure 3. Ball and stick representations of two isomers deriving from the [Mo$_2$O$_2$S$_2$(nta)$_2$]$^{4-}$ complex, (a) cis isomers (**1b**) observed in the adduct {**1a**−**1b**}; (b) trans isomer (**1b′**) characterized in the compound **3**.

bridges.[20] The central cluster [Mo$_3$S$_4$(nta)$_3$]$^{5-}$ is anchored to the {Mo$_{18}$} macrocycle by its three carboxylate arms, each spanning two adjacent Mo atoms. These three carboxylate groups are nearly located in plane of the ring, while the {Mo$_3$S$_4$} core is found out of plane as a ring-capping group (see Figure 1b). Nine inner aquo ligands are distributed as three bridging and six terminal molecules, which interact with the vicinal carboxylate groups through H-bonds (O···O = 2.675(7)−2.766(7) Å). The host guest assembly **1a** exhibits a "heart-shape" conformation with an idealized C_{3v} symmetry. Bond lengths and angles fall in the usual range observed for such arrangements.[3,4] In the solid state, both discrete clusters **1a** and **1b** interact mutually to give a striking supramolecular assembly (see Figure 2). The {Mo$_{18}$} ring associated to the {Mo$_3$S$_4$}-based complex (**1a**) acts as a widened open basket where the guest component [Mo$_2$O$_2$S$_2$(nta)$_2$]$^{4-}$ (**1b**) appears to be grafted on the hydrophilic surface of the cavity through two short H-bonds involving both hanging carboxylate groups of **1b** and two hydroxo bridges of **1a** (O···O = 2.586(8)−2.601(8)Å). In addition, three potassium ions were found within the pocket, interacting mainly with inner aquo ligands and water molecules (K−O = 2.7−3.1 Å). The presence of these potassium ions closely embedded within holes of the ring should probably favor the H-bond interactions between both anionic units **1a** and **1b**, by decreasing the anionic charge of the overall molecular assembly.

trans-[Mo$_2$O$_2$S$_2$(Hnta)$_2$]$^{2-}$ (1b′, Compound 3). The structure of the anion **1b′** derives structurally from **1b**. The single dinuclear unit {Mo$_2$O$_2$S$_2$} contains two nitrilotriacetate groups coordinated to the Mo centers, but the relative disposition of both nitrilotriacetato ligands reveals a trans isomer characterized by its two opposite carboxylates. The complex **1b′** is chiral (C_2 idealized symmetry), but in the solid state, both enantiomers are related together by a gliding mirror plane to give a racemic crystal. It is worth noting that **1b**, previously reported as an isolated compound[21] and here as a subcomponent in **1** (see above), corresponds to the cis isomer (see Figure 3). Bond-length analysis reveals that both hanging carboxylate groups in **1b′** are protonated (C−OH = 1.321(8)−1.308(9) Å and C=O = 1.212(8)−1.206(9) Å).

Behavior in Solution. Supramolecular assembly {**1a**−**1b**} in compound **1** has been characterized in D$_2$O and DMSO[d_6] by multi-^{1}H NMR experiments (1D, COSY, NOESY, and DOSY). Comparison of the ^{1}H NMR data of {**1a**−**1b**} with those of the individual species **1a** (compound **2**) and **1b′** (compound **3**) gives

---

(20) The bond valence sum calculation (BVS) for the bridging oxygen atoms supports this view. BVS mean value of 1.19 ± 0.07 (1.28 and 1.02 for the maximum and minimum BVS values, respectively) is consistent with hydroxo groups.

(21) Wu, J.-F.; Li, D.-M.; Cui, L.-F.; Zhuang, C.-F.; Song, S.-N.; Wang, T.-G.; Xu, J.-Q.; Jia, H.-Q.; Hu, N.-H. *Appl. Organomet. Chem.* **2007**, *21*, 1033.

Table 2. ^{1}H NMR Data Related to the Resonances of the nta^{3-} Ligand in Na$_2$[Mo$_3$S$_4$(Hnta)$_3$]·7H$_2$O, **1**, **2**, and **3** in D$_2$O at 298 K

compounds	molecular unit	peak label	^{1}H NMR data δ/ppm (multiplicity, $\Delta\nu_{1/2}$/Hz)
Na$_2$[Mo$_3$S$_4$(Hnta)$_3$]·7H$_2$O			5.39 (6H,3),
			4.73 (12H,4)
2≡Cs$_{4.7}$(NMe$_4$)$_{0.3}$-1a·36H$_2$O	**1a**	D1	3.80 (6H,8)
		D2	3.49 (6H,8)
		S1	3.39 (6H,10)
1≡K$_9$-{1a−1b}·45H$_2$O	**1a**	D1	3.83 (6H,6)
		D2	3.47 (6H,50)
		S1	3.69 (6H,8)
	1b	d1	4.40 (2H,6)
		d2	4.38 (2H,7)
		d3	4.18 (2H,9)
		d4	3.94 (2H,6)
		d5	3.78 (2H,14)
		d6	3.51 (2H,14)
3≡KNa-1b′·7H$_2$O	**1b′**		4.82 (4H,75),
			4.54 (4H,55),
			4.39 (4H,50)
	1b		4.16 (4H,55),
			3.98 (4H,30),
			3.97 (4H,85)

Table 3. ^{1}H NMR Data Related to the Hydroxo Resonances of the {Mo$_{18}$} Ring in **1** and **2** in DMSO at 298 K

compounds	^{1}H NMR data δ/ppm (multiplicity)
2≡Cs$_{4.7}$(NMe$_4$)$_{0.3}$-1a·36H$_2$O	10.92 (3H), 10.66 (3H), 10.42 (6H), 10.30 (6H)
1≡K$_9$-{1a−1b}·45H$_2$O	10.93 (3H), 10.67 (3H), 10.43 (6H), 10.38 (6H)

strong arguments to state the supramolecular system {**1a−1b**} is retained through weak hydrogen bonds in a polar solvent such as D$_2$O or DMSO. Relevant NMR data are given in Tables 2 and 3. First, immobilization of the [Mo$_3$S$_4$(nta)$_3$]$^{5-}$ complex within the {Mo$_{18}$} ring is evidenced by ^{1}H NMR features (see Figure 4). Initially, in D$_2$O, uncoordinated [Mo$_3$S$_4$(nta)$_3$]$^{5-}$ gives two signals with a 2:1 intensity ratio, consistent with the presence of two distinct methylene groups, one corresponding to the six attached acetates (4.73 ppm, 12H) and the other to the three hanging acetate arms (5.39 ppm, 6H), respectively. Such a distribution is consistent with an average environment for the protons of the attached acetate resulting from rapid rotation motion along the involved σ bonds. The anchorage of the three hanging carboxylate arms within the {Mo$_{18}$} ring provokes the splitting of the 12H signal into two doublets at 3.80 and 3.49 ppm labeled D1 and D2, respectively. Such a situation agrees with a frozen conformation for these acetate groups on the NMR time scale. In addition, the resonance pattern of three hanging acetates (singlet labeled S1 at 3.39 ppm) remains unaffected for symmetry reasons, each of these three methylene groups being crossed by a mirror plane. The conformational freeze of the three nta ligands through the encapsulation of the [Mo$_3$S$_4$(nta)$_3$]$^{5-}$ complex is also observed by a systematic broadening of the methylene resonances from about 3−4 Hz to 8−10 Hz. Two-dimensional (2D) COSY and NOESY ^{1}H NMR of **1a** (compound **2**) (see Figures S2 and S3 in Supporting Information) confirm the scalar coupling between these diastereotopic protons ($^2J_{H-H}$ = 16 Hz) and the close nearness of the three distinct methylene groups (H···H ≈ 2.25−2.27 Å), respectively. Furthermore, encapsulation of
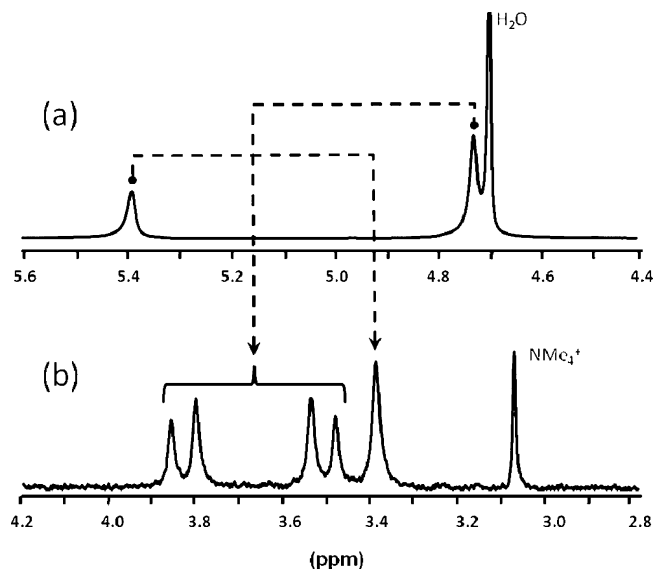
Figure 4. ^{1}H NMR spectrum of {Mo$_3$S$_4$(Hnta)$_3$} moeity in D$_2$O showing the resonances of the methylene groups of the {nta} ligands (a) within uncoordinated [Mo$_3$S$_4$(Hnta)$_3$]$^{2-}$ and (b) within [Mo$_3$S$_4$(nta)$_3$]$^{5-}$⊂-{Mo18} (**1a**). Dotted arrows feature the variations of the chemical shifts and the patterns of the resonances through the encapsulation of the {Mo$_3$S$_4$(Hnta)$_3$} cluster.
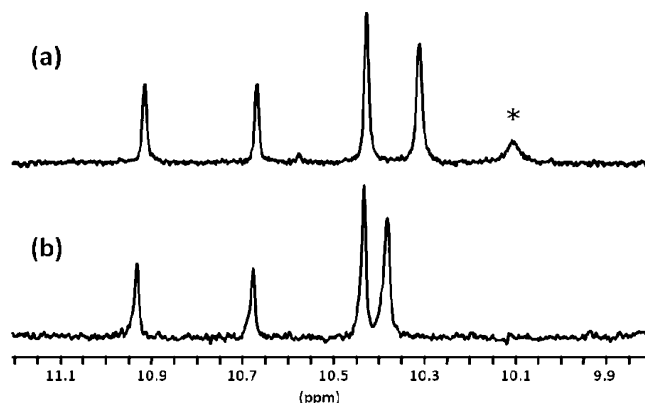
Figure 5. ^{1}H NMR spectra of compounds **1a** (top) and {**1a−1b**} (bottom) in DMSO showing the resonances of the hydroxo groups of the {Mo$_{18}$} inorganic ring (* = unidentified impurity).

[Mo$_3$S$_4$(nta)$_3$]$^{5-}$ within the {Mo$_{18}$} ring produces the typical shielding on the ^{1}H nuclei,[3−7] larger for the *in-plane* methylene of the anchoring acetate located in the {Mo$_{18}$} averaged plane ($\Delta\delta$ = −2.0 ppm) and significantly less pronounced ($\Delta\delta$ = −0.9 and −1.2 ppm) for the six *out-of-plane* acetates coordinated to the {Mo$_3$S$_4$} moiety. In DMSO, the ^{1}H NMR spectrum of **1a** (Figure 5a) exhibits four high-frequency resonances between 10−11 ppm with 1:1:2:2 intensity ratios, corresponding to the 18 hydroxo bridges engaged in the C_{3v} symmetry ring (see Table 3).

The ^{1}H NMR spectrum of the {**1a−1b**} system (compound **1**) in DMSO[d_6] shown in Figure 5b (hydroxo region) is similar to that of the individual species **1a** and consists of four resonances in agreement with the presence of the 18 hydroxo groups involved within a C_{3v} {Mo$_{18}$} ring (see Table 3). In D$_2$O, the methylene resonances of the nta^{3-} ligands in {**1a−1b**} give rise to a complex ^{1}H spectrum, which has been interpreted and satisfyingly modeled considering two subspectra related to the presence of both molecular entities **1a** and **1b**. The experimental ^{1}H NMR spectra for 10^{-3} mol·L^{-1} and 2.1 × 10^{-2} mol·L^{-1} in
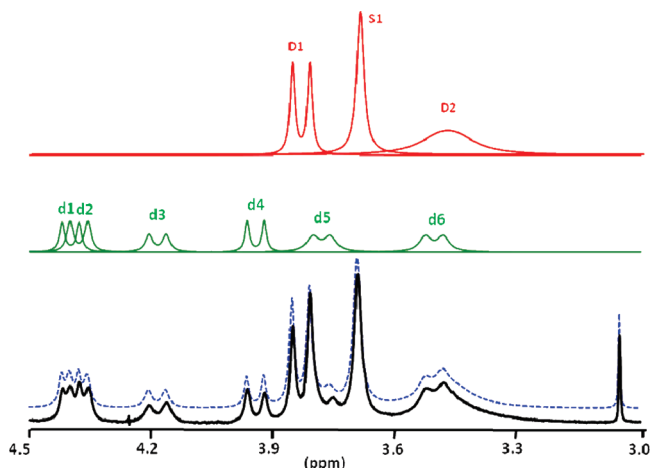
Figure 6. ^{1}H NMR spectrum of the supramolecular adduct {**1a**−**1b**} (10^{-3} mol·L^{-1} in D$_2$O) (black line) is analyzed as two subspectra which correspond to the **1b** (green line) and to the **1a** subunits (red line). The sum of the two simulated subspectra is represented as a dotted blue line.

{**1a**−**1b**}, superimposed with the two simulated subspectra, are shown in Figures 6 and S4 in Supporting Information, respectively. The subunit **1b** is characterized by six equal and narrow doublets ($^2J_{H-H} = 17$ Hz, labeled from d1 to d6 and presented in Table 2). They correspond to the six diastereotopic protons belonging to the three kinds of methylene groups of the two equivalent nta^{3-} ligands. Then, each doublet d1−d6 corresponds to a 2H intensity. The other subcomponent of the spectrum assigned to the **1a** moiety consists of three equal 6H signals distributed as a resolved doublet ($^2J_{H-H} = 17$ Hz) centered at 3.83 ppm (labeled D1), a singlet at 3.69 ppm (labeled S1), and a broad resonance at 3.47 ppm corresponding to the unresolved doublet D2. The 2D COSY spectrum of {**1a**−**1b**} supports entirely these assumptions, owing to the establishment of the scalar connectivities between the doublets d1−d4, d2−d6, and d3−d5 for **1b** and D1−D2 for **1a** (shown in Figure S5 in Supporting Information). In addition, the 2D NOESY spectrum of {**1a**−**1b**} exhibits the expected spatial connectivities and/or proximities (i) between the six doublets d1−d6 from **1b**, (ii) between the three D1, D2, and S1 resonances from **1a** (see Figure S6 in Supporting Information). In addition, the ^{1}H NMR spectrum of {**1a**−**1b**} exhibits a significant temperature dependence between 280 and 320 K (see Figure S7 in Supporting Information). As the temperature increases, the six doublets d1−d6 broaden but still remain present at 320 K. Conversely, the three signals attributed to **1a** sharpen until the D2 doublet is resolved.

It is worth noting that the presence of the **1b** entity affects significantly the ^{1}H NMR pattern of **1a**. The S1 chemical shift varies of about 0.3 ppm, while the D2 line-width increases substantially from 8 to 50 Hz (see Table 3). Moreover, the presence of the six sharp doublets d1−d6 indicates that the overall CH$_2$ rotations are hindered in **1b**, including even those of the hanging carboxylate groups expected to be more flexible and labile than those of the coordinated nta ligands. This result is consistent with the solid-state structure of **1b** and suggests that a frozen arrangement could be preserved through the supramolecular interactions within {**1a**−**1b**}.

Surprisingly, such a situation appears significantly different to that observed with the individual species **1b**′ (compound **3**), which structurally derives from **1b**. Compound **3** in D$_2$O at 300 K gives four broad poorly resolved asymmetric signals, which
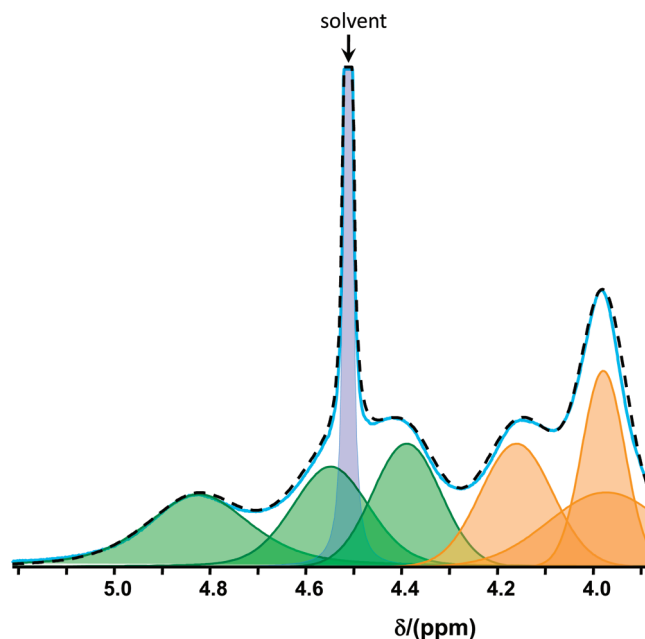

Figure 7. ^{1}H NMR spectrum of the *trans*-[Mo$_2$O$_2$S$_2$(Hnta)$_2$]$^{2-}$ (**1b**′) at 300 K (blue line), consisting of two sets of three equal broad signals related to an isomerization process between *trans*-**1b**′(green lines) and *cis*-**1b** (orange lines). The sum of the two subspectra (green and orange) gives the dotted black line (* = uncoordinated nta^{3-} ligand which represents less than 5%).

fit satisfyingly with six equal resonances (see Figure 7). Such features, i.e broadness and peak distribution, suggest that a dynamic cis/trans equilibrium (**1b**′ ⇌ **1b**) take place in solution. Then, each broad line should be assigned reasonably to the averaged resonances of the two protons of each methylene group. As each isomer contains three nonequivalent methylene groups, the cis/trans mixture in an equal ratio should produce six equal resonances, distributed as two sets of three resonances, consistent with the simulated and experimental data. Furthermore, the three lines corresponding to the cis isomer (**1b**) should result from the averaged signals of the three pairs of coupled doublets d1−d4, d2−d6, and d3−d5, previously observed for the cis isomer in a frozen conformation in {**1a**−**1b**}. The mean values calculated for these three pairs of doublets are 4.17, 3.95, and 3.98 ppm, which differ less than 0.02 ppm from the three low-frequency peaks at 4.16, 3.97, and 3.98 ppm. From these considerations, the three high-frequency resonances at 4.82, 4.54, and 4.39 ppm can be tentatively assigned to the trans isomer (**1b**′) while the other three attributed to the cis isomer (**1b**) (see Table 2). Variable temperature ^{1}H NMR experiment in D$_2$O recorded in the 275−345 K range (see Figure 8) supports such an interpretation. Temperature decreasing until 275 K produces significant narrowing of the lines that leads to a splitting into two components for two of them. Conversely, the temperature increasing up to 345 K provokes the coalescence of several lines to give three broad resonances with almost equal intensities observed at 5.15, 4.92, and 4.57 ppm. These results indicate that in such conditions, both isomers are in a situation of fast exchange on the NMR time scale, leading to an averaged cis/trans environment for the three distinct methylene groups of the coordinated Hnta^{2-} ligands i.e. axial, equatorial and hanging. At last, the variable temperature ^{1}H NMR feature of compound **3** exhibits weak dependence upon pH. Nevertheless, the most important result of this work is definitely the striking behavior of the dinuclear unit [Mo$_2$O$_2$S$_2$(nta)$_2$]$^{4-}$ in the presence of the
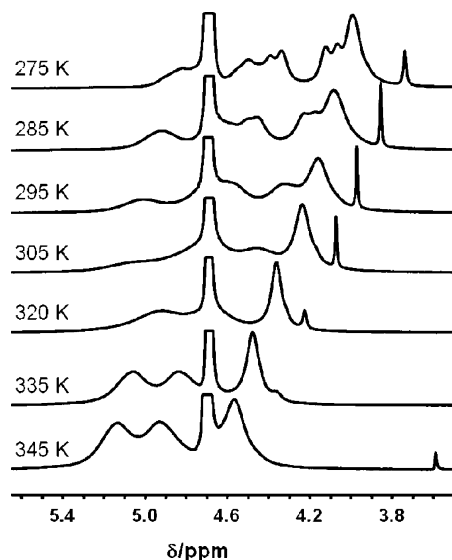
Figure 8. Variable-temperature ^{1}H NMR spectra of compound **3** in D$_2$O.

Table 4. Diffusion Coefficient in D$_2$O and Molecular Mass of the Compounds

compounds	D /μm$^2\cdot$s^{-1}	molecular mass/g·mol^{-1}
[Mo$_2$O$_2$S$_2$(Hnta)$_2$]$^{2-}$, **1b**	408	666.6
[Mo$_3$S$_4$(Hnta)$_3$]$^{2-}$	389	983.5
[Mo$_{18}$(Mo$_3$S$_4$(nta)$_3$)]$^{5-}$, **1a**	259	4036.8
[Mo$_{18}$(Mo$_3$S$_4$(nta)$_3$)][Mo$_2$O$_2$S$_2$(nta)$_2$]$^{9-}$, {**1a−1b**}	240	4836.0
[Mo$_{12}$Trim]$^{3-a}$	315	2139.3
[Mo$_{16}$(IsoP)$_2$]$^{4-a}$	295	2940.5
[Mo$_{16}$(PDA)$_2$]$^{4-a}$	279	3032.6

^{a} The values of self-diffusion coefficients D for these compounds come from ref 26.

offer a powerful tool to characterize dynamic entities in solution and were successfully applied for the characterization of biological or supramolecular systems in solution,[23] such as proteins, ion pairs,[24] or polymetallic coordination complexes.[25] The DOSY NMR technique has proved to be useful to characterize the templated-oxothiomolybdenum rings,[4,7,26] which constitute an ideal series of quasi-circular hollow systems. In the present study, the ^{1}H NMR resonances of the methylene groups of the coordinated nitrilotriacetate ligands were used to perform the DOSY experiments on the individual species [Mo$_3$S$_4$(Hnta)$_3$]$^{2-}$, [Mo$_2$O$_2$S$_2$(Hnta)$_2$]$^{2-}$ in compound **3**, the host−guest complex **1a** and the supramolecular adduct {**1a−1b**}. The self-diffusion coefficients (D) and the corresponding calculated molecular masses (MM) are given in Table 4, which include additional data of characteristic templated oxothiomolybdenum rings with nuclearity ranging from Mo$_{12}$ to Mo$_{16}$. The isolated components [Mo$_3$S$_4$(Hnta)$_3$]$^{2-}$ and [Mo$_2$O$_2$S$_2$(Hnta)$_2$]$^{2-}$ exhibit the highest self-diffusion coefficients ($D = 389$ μm$^2\cdot$s^{-1} and $D = 408$ μm$^2\cdot$s^{-1}, respectively) related to their small size while that of the {Mo$_{18}$}-based anion (**1a**) is significantly smaller ($D = 259$ μm$^2\cdot$s^{-1}). Interestingly, the species **1a** and **1b** within the adduct {**1a−1b**} give the same value $D = 240$ μm$^2\cdot$s^{-1} (see Figure 9), indicating that both components **1a** and **1b** are traveling together through a unique diffusion process. This is still consistent with the overall results presented above, which confirm that assembly {**1a−1b**} exists in aqueous solution even at low concentration (below 10^{-3} M) and until 320 K. Besides, the plot log D versus log MM for a large series of hollow compounds, including templated-{Mo$_n$} anions, some crown-ethers, and the nanoscale Keplerate anion (noted {Mo$_{132}$})[27] is found to be quite linear (see Figure S9 in Supporting Information), meaning that the molecular volume V_m is almost constant to give a unified relationship for this series

[Mo$_3$S$_4$(nta)$_3$]$^{5-}$-templated {Mo$_{18}$} ring (**1a**). The 12 sharp lines, distributed as six doublets, indicate that the dimeric complex adopts a single frozen arrangement consistent with the solid-state cis isomer. Alternatively, in {Mo$_{18}$}-free solutions, the variable-temperature ^{1}H NMR spectra of the trans dimer (**1b′**) are fully consistent with a dynamic cis/trans equilibrium, giving broad temperature-dependent resonances. Besides, a synthetic mixture containing initially **1a** and **1b′** (trans isomer) in a 1:1 stoichiometric ratio at pH = 4.5 in D$_2$O allows recovery of the ^{1}H NMR spectrum of the adduct {**1a−1b**} (see Figure S8 in Supporting Information). In spite of the low concentrated sample (about 7 × 10^{-4} mol·L^{-1}), four doublets among the six and the specific broadening of D2 were observed, previously attributed to the specific interaction **1a···1b**. It means that specific H-bond interactions arising from the {Mo$_{18}$} cycle generate supramolecular reactivity able to convert quantitatively the *trans*-**1b′** into the *cis*-**1b** isomer.

Further arguments allow to state that weak interactions in {**1a−1b**} are retained in solution (DMSO or H$_2$O). As previously mentioned, ^{1}H NMR spectra of **1a** and {**1a−1b**} in DMSO (see Figure 5) exhibit similar peak distribution in the region of the bridging hydroxo groups of the {Mo$_{18}$} ring in a C_{3v}-observed symmetry. On comparative examination of both spectra, three resonances appear quite unaffected by the presence of **1b** and differ by less than 0.01 ppm, while the 10.30 ppm line (6H) observed in **1a** shifts significantly to 10.38 ppm in {**1a−1b**}($\Delta\delta$ = 0.08 ppm). This result indicates that among the 18 hydroxo bridges, only six distributed on one side of the wheel are able to be engaged in the H-bond interactions with the dinuclear unit **1b**, producing the expected deshielding effect at these H nuclei.[22] Besides, the unchanged averaged C_{3v} symmetry means that the supramolecular association {**1a−1b**} exists as a labile and dynamic complex where the dinuclear unit **1b** is able to rock and roll over one side of the surface of the {Mo$_{18}$}. A definitive argument can be given to confirm the retention of the supramolecular adduct in aqueous solution. Diffusion NMR methods

(22) (a) Steiner, T. *Angew. Chem., Int. Ed.* **2002**, *41*, 48. (b) Jeffrey, G. A. *An Introduction to Hydrogen Bonding*; Oxford University Press: Oxford, 1997. (c) Eckert, H.; Yesinowski, J. P.; Silver, L. A.; Stolper, E. M. *J. Phys. Chem.* **1988**, *92*, 2055.

(23) (a) Gostan, T.; Tramesel, D.; Brun, E.; Prigent, Y.; Delsuc, M. A. *Spectra Anal.* **2004**, *33*, 26. (b) Gilard, V.; Trefi, S.; Balayssac, S.; Delsuc, M. A.; Gostan, T.; Malet-Martino, M.; Martino, R.; Prigent, Y.; Taulelle, F. In *NMR Spectroscopy in Pharmaceutical Analysis*; Holzgrabe, U., Wawer, I., Diehl, B., Eds.; Elsevier: Dordrecht, 2008; pp 269−289. (c) Gostan, T.; Moreau, C.; Juteau, A.; Guichard, E.; Delsuc, M. A. *Magn. Reson. Chem.* **2004**, *42*, 496.

(24) Martinez-Viviente, E.; Pregosin, P. S.; Vial, L.; Herse, C.; Lacour, J. *Chem.—Eur. J.* **2004**, *10*, 2912.

(25) (a) Terazzi, E.; Torelli, S.; Bernadinelli, G.; Rivera, J. P.; Bénech, J.-M.; Bourgogne, C.; Donnio, B.; Guillon, D.; Imbert, D.; Bünzli, J.-C. G.; Pinto, A.; Jeannerat, D.; Piguet, C. *J. Am. Chem. Soc.* **2005**, *127*, 888. (b) Greenwald, M.; Wessely, D.; Golberg, I.; Cohen, Y. *New J. Chem.* **1999**, *23*, 337. (c) Fernandez, I.; Martinez-Viviente, E.; Pregosin, P. S *Inorg. Chem.* **2005**, *44*, 5509.

(26) Floquet, S.; Brun, S.; Lemonnier, J.-F.; Henry, M.; Delsuc, M.-A.; Prigent, Y.; Cadot, E.; Taulelle, F. *J. Am. Chem. Soc.* **2009**, *131*, 17254.

(27) Müller, A.; Krickemeyer, E.; Bogge, H.; Schmidtmann, M.; Peters, F. *Angew. Chem., Int. Ed.* **1998**, *37*, 3360.
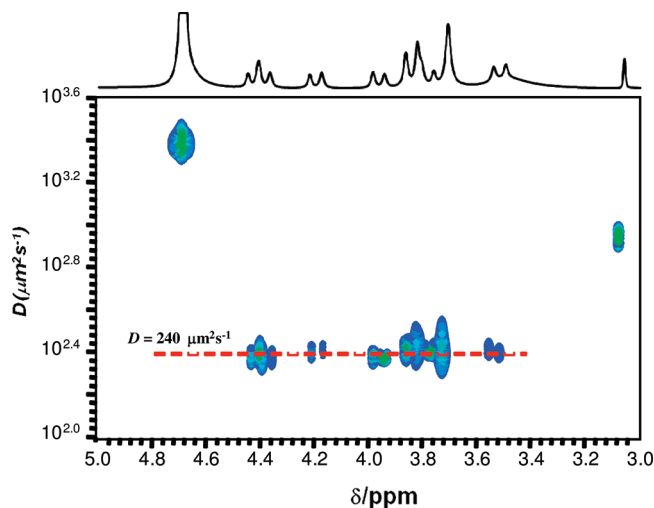
Figure 9. Two-dimensional diffusion spectrum of {**1a**−**1b**} adduct highlighting the same D value for both subcomponents $[Mo_2O_2S_2(nta)_2]^{4-}$ (**1b**) and $[Mo_3S_4(nta)_3]^{5-} \subset \{Mo_{18}\}$ (**1a**).

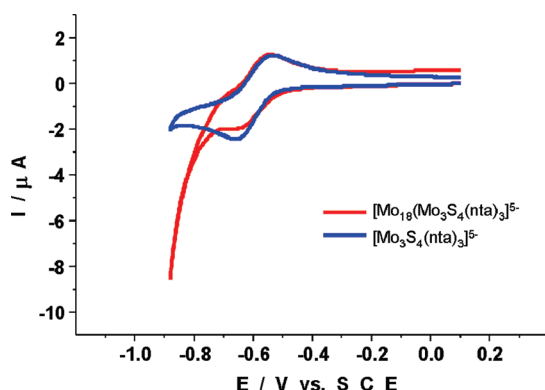**Figure 10.** Cyclic voltammograms of 1 mM solutions of **1a** and $[Mo_3S_4(nta)_3]^{5-}$ in a pH 7 medium (0.5 M Li_2SO_4 + 0.2 M tris(hydroxymethylaminomethane) + H_2SO_4). The scan rate was 10 mV s^{-1}, using glassy carbon and SCE as working and reference electrodes, respectively.

between the self-diffusion coefficient and the molecular mass *MM*. This correlation ($\log D = -0.345 \ln MM + 3.657$) gives the molecular masses $MM = 3997.6$ and $MM = 4984.5$ g·mol^{-1} for **1a** and {**1a**−**1b**}, respectively. These results appear to be in good agreement with those calculated from X-ray diffraction analysis (see Table 4).

Electrochemical Studies. The cyclic voltammograms (CVs) of **1a** and $[Mo_3S_4(nta)_3]^{5-}$ recorded in pH 7 buffer display a chemically reversible couple assigned to the formation of the first reduction state of the $\{Mo_3S_4\}$ cluster (see Figure 10). The redox potentials E^0 (mean values between the cathodic and anodic peak potentials) are very close for the two compounds (~ -0.6 V vs SCE). The E^0 values correspond to that previously reported for the one-electron reduction process of $[Mo_3S_4\text{-}(nta)_3]^{5-}$.[10] However, some differences between both CVs are observed: (i) With the complex **1a**, a positive shift of 50 mV is measured for the onset potential of the faradaic current; (ii) the anodic to cathodic peak potential differences (ΔE_p) are 0.110 V for **1a** and 0.120 V for $[Mo_3S_4(nta)_3]^{5-}$. These observations indicate slightly more favorable kinetics of electrochemical reactions in the case of **1a**. Between -0.850 and -1 V (vs SCE), a large plurielectronic irreversible wave appears in the CV of **1a** which was not present in that of $[Mo_3S_4(Hnta)_3]^{2-}$ (Figure S10 in Supporting Information). This wave is assigned to the

reduction of Mo^V centers. In the positive potential domain vs SCE, the Mo centers are associated with a broad plurielectronic irreversible oxidation wave with a peak around 1.1 V vs SCE (not shown).

The variation of the first reduction peak current intensity of **1a** is linear as a function of the square root of the scan rate (Figure S11). The linearity of this curve indicates that the CV of **1a** features a diffusion-controlled process. The same observation was also been made with $[Mo_3S_4(Hnta)_3]^{2-}$ under similar conditions. Furthermore, the ratio of the peak current intensity of **1a** to that of $[Mo_3S_4(nta)_3]^{5-}$ (Ipc^a/Ipc^b = 0.81) is nearly equal to the ratio $(D^a/D^b)^{1/2}$, where D^a and D^b are the diffusion coefficients of **1a** and $[Mo_3S_4(nta)_3]^{5-}$ determined by DOSY NMR, respectively.[28] It has been reported[10] that the cyclic voltammetric pattern of $[Mo_3S_4(Hnta)_3]^{2-}$ exhibits three successive one-electron processes in alkaline medias (pH range 8 to 11.1). However, bulk controlled potential coulometries carried out at -0.630 V versus SCE (i.e., first reduction process) in the pH 7 medium indicate that the consumption of electrons exceeds 1 electron per molecule for $[Mo_3S_4(Hnta)_3]^{2-}$ and **1a**. For example, controlled potential coulometry was stopped after the consumption of 88% and 86% of the initial current respectively for $[Mo_3S_4(Hnta)_3]^{2-}$ and **1a**. In these conditions, the corresponding consumed electrons were roughly 1.6 and 5.9 electrons per molecule for $[Mo_3S_4(Hnta)_3]^{2-}$ and **1a**, respectively. Interestingly, the consumed electrons could not be fully recovered after reoxidation carried out at $+0.1$ V versus SCE. Actually, only roughly 32% and 14% of the consumed electrons were recovered respectively for $[Mo_3S_4(Hnta)_3]^{2-}$ and **1a**. Such behavior, already observed with other polyoxometalates,[29] could be due to catalytic and/or decomposition processes. However, the various CVs run at different advancement stages of the electrolyses have permitted ruling out any significant decomposition processes of the complexes. Alternatively, catalysis of the hydrogen evolution reaction by the third reduction process of $[Mo_3S_4(Hnta)_3]^{2-}$ has been reported in alkaline solutions.[10] The hydrogen evolution reaction was also observed with Mo−S-based complexes,[8] or $\{Mo_3S_4\}^{4+}$ modified electrode surfaces[30] and other polyoxometalates dissolved in various media.[31] Our controlled potential coulometry observations might, therefore, be mainly explained by similar HER catalytic reactions, promoted either by inner $\{Mo_3S_4\}$ core, by Mo_{18}-ring, or both.

In support of this scheme, the voltammetric waves are gradually obscured by the catalytic wave, as the pH decreases, thus underscoring an enhanced catalysis in media of higher acidity (Figure S12 in Supporting Information). In the present study, we show that such a process is efficient enough to be

(28) Bard, A. J.; Faulkner, L. R. *Electrochemical Methods: Fundamentals and Applications*; Wiley: New York, 1980; p 213.

(29) (a) Keita, B.; Nadjo, L. In *Electrochemical Reactions on Modified Electrodes*; Bard, A. J., Stratmann, M., Eds.; Encyclopedia of Electrochemistry, Vol. 10; Wiley-VCH: New York, 2007; p 685. (b) Hussain, F.; Kortz, U.; Keita, B.; Nadjo, L.; Pope, M. T. *Inorg. Chem.* **2006**, *45*, 761. (c) Lisnard, L.; Mialane, P.; Dolbecq, A.; Marrot, J.; Clemente-Juan, J.-M.; Coronado, E.; Keita, B.; de Oliveira, P.; Nadjo, L.; Sécheresse, F. *Chem.−Eur. J.* **2007**, *13*, 3525.

(30) Jaramillo, T. F.; Bonde, J.; Zhang, J.; Ooi, B.-L.; Andersson, K.; Ulstrup, J.; Chorkendorff, I. *J. Phys. Chem. C* **2008**, *112*, 17492.

(31) A short list of pioneering papers includes: (a) Savinov, E. N.; Saidkhanov, S. S.; Parmon, V. N.; Zammarev, K. I. *React. Kinet. Catal. Lett.* **1981**, *17*, 407. (b) Ioannidis, A.; Papaconstantinou, E. *Inorg. Chem.* **1985**, *24*, 439. (c) Akid, R.; Darwent, J. *J. Chem. Soc., Dalton Trans.* **1985**, 395. (d) Keita, B.; Nadjo, L. *J. Electroanal. Chem.* **1987**, *217*, 287.

observed early on the first one-electron process (above −1 V vs SCE) in neutral or slightly acidic pH media.

Conclusion

In summary, we have discovered a new type of nanoscale $\{Mo_2O_2S_2\}$-based cycle by use of the complexe $[Mo_3S_4-(Hnta)_3]^{2-}$ as structuring agent, which allowed isolation of the $\{[Mo_3S_4(nta)_3]^{5-}\subset\{Mo_{18}\}\}$ macrocycle (**1a**). Structural characterizations of crystals showed that the targeted prototype is combined to a dinuclear complex $\{Mo_2O_2S_2\}$ coordinated to two nta^{3-} ligands arranged in a cis fashion (**1b**). In the solid state, such association $\{\mathbf{1a}-\mathbf{1b}\}$ is maintained by two short H-bonds involving the hanging carboxylate groups of the nta ligands in **1b** and two hydroxo bridges of the $\{Mo_{18}\}$ cycle (**1a**). This result was explained by structural reorganizations, occurring during the crystallization process and favored by the presence of potassium ion, whereas the $\{Mo_{18}\}$-based ring can be obtained pure through fast precipitation using Cs$^+$ cation. Multiexperiment ^{1}H NMR studies (1D, COSY, NOESY, DOSY) have demonstrated that the large $\{Mo_{18}\}$-based assembly is stable in polar solvents such as water or DMSO, though the most remarkable behavior is undoubtedly the retention of the supramolecular assembly $\{\mathbf{1a}-\mathbf{1b}\}$ in such polar solvents while dissociation involving solvent molecules should be readily expected. Such unusual behavior can be related to the intimate properties of these cyclic materials where supramolecular stability must not be understood by only two H-bonds as depicted in the solid state, but to a certain extent by a dynamic H-bond network involving mainly six hydroxo groups present on one side of the $\{Mo_{18}\}$, allowing both subcomponents to associate together as a labile assembly. In this way, the encapsulation of the $\{Mo_3S_4\}$ cluster within oxothiomolybdenum cyclic materials gives access to large multicomponent systems able to cumulate (supra)chemical or electrochemical properties at the molecular level. New properties or functions can be precisely targeted from this molecular platform. The nuclearity of the host could be tuned by changing the length of the three hanging alkyl-carboxylate arms, while the electrochemical and/or coordinative properties of the $\{Mo_3S_4\}$ embedded cluster can be drastically changed by reacting with electron-rich metallic atoms such as Pd, Ni, Fe etc... In the future, we are looking to develop electrocatalysts from this new class of molecular systems.

Supporting Information Available: UV−visible spectra of **1a** in pH 7 buffer medium (Figure S1); 2D COSY spectrum of **1a** in D$_2$O (Figure S2); 2D NOESY spectrum of **1a** in D$_2$O (Figure S3); ^{1}H NMR spectrum of **1** in D$_2$O (2.1×10^{-2} mol·L^{-1}) (Figure S4); 2D COSY spectrum of $\{\mathbf{1a}-\mathbf{1b}\}$ in D$_2$O (2.1×10^{-2} mol·L^{-1}) (Figure S5); 2D NOESY spectrum of **1a** in D$_2$O (2.1×10^{-2} mol·L^{-1}) (Figure S6); variable-temperature ^{1}H NMR study of $\{\mathbf{1a}-\mathbf{1b}\}$ in D$_2$O (Figure S7); 1D ^{1}H NMR spectrum of stoichiometric mixture of **1b'** (compound **3**) and **1a** in D$_2$O (7×10^{-4} mol·L^{-1}) (Figure S8); linear correlation log D vs log MM for hollow cycles and spheres (Figure S9); cyclic voltammograms of **1a** and $[Mo_3S_4(nta)_3]^{5-}$ in a pH 7 medium (Figure S10); peak current intensity variations as a function of the square root of scan rate for **1a** in a pH 7 medium (Figure S11); CVs of **1a** in pH 7 and pH 5 buffers (Figure S12). This material is available free of charge via the Internet at http://pubs.acs.org.

JA909762P